Environmental Pollution 275 (2021) 116544

Contents lists available at ScienceDirect

Environmental Pollution

journal homepage: www.elsevier.com/locate/envpol

Black carbon concentration in the central Himalayas: Impact on glacier melt and potential source contribution☆

Chaman Gul [a, b, c, d], Parth Sarathi Mahapatra [a], Shichang Kang [b, d, e], Praveen Kumar Singh [a, f], Xiaokang Wu [g], Cenlin He [h, i], Rajesh Kumar [i], Mukesh Rai [a, b, d], Yangyang Xu [g], Siva Praveen Puppala [a, *]

[a] International Centre for Integrated Mountain Development (ICIMOD), GPO Box 3226, Kathmandu, Nepal
[b] State Key Laboratory of Cryospheric Sciences, Northwest Institute of Eco-Environment and Resources, Chinese Academy of Sciences, Lanzhou, 73000, China
[c] Reading Academy, Nanjing University of Information Science and Technology, Nanjing, Jiangsu, 210044, China
[d] University of Chinese Academy of Sciences, Beijing, China
[e] CAS Centre for Excellence in Tibetan Plateau Earth Sciences, Beijing, 100101, China
[f] Centre of Excellence in Disaster Mitigation and Management, Indian Institute of Technology Roorkee, Roorkee, Uttarakhand, 247667, India
[g] Department of Atmospheric Sciences, Texas A&M University, College Station, TX, 77843, USA
[h] Advanced Study Program and Research Applications Laboratory, National Center for Atmospheric Research, Boulder, CO, 80301, USA
[i] Research Applications Laboratory, National Center for Atmospheric Research, 1850 Table Mesa Dr, Boulder, CO, 80305, USA

ARTICLE INFO

Article history:
Received 2 December 2019
Received in revised form
13 January 2021
Accepted 16 January 2021
Available online 23 January 2021

Keywords:
Hindu Kush Himalaya
Yala glacier
WRF-CHEM simulations
SNICAR
Source studies
Black carbon

ABSTRACT

This study discusses year-long (October 2016–September 2017) observations of atmospheric black carbon (BC) mass concentration, its source and sector contributions using a chemical transport model at a high-altitude (28°12′49.21″N, 85°36′33.77″E, 4900 masl) site located near the Yala Glacier in the central Himalayas, Nepal. During a field campaign, fresh snow samples were collected from the surface of the Yala Glacier in May 2017, which were analysed for BC and water-insoluble organic carbon mass concentration in order to estimate the scavenging ratio and surface albedo reduction. The maximum BC mass concentration in the ambient atmosphere (0.73 μg m^{-3}) was recorded in the pre-monsoon season. The BC and water-insoluble organic carbon analysed from the snow samples were in the range of 96–542 ng g^{-1} and 152–827 ng g^{-1}, respectively. The source apportionment study using the absorption Ångström exponent from in situ observations indicated approximately 44% contribution of BC from biomass-burning sources and the remainder from fossil-fuel sources during the entire study period. The source contribution study, using model data sets, indicated ~14% contribution of BC from open-burning and ~77% from anthropogenic sources during the study period. Our analysis of regional contributions of BC indicated that the highest contribution was from both Nepal and India combined, followed by China, while the rest was distributed among the nearby countries. The surface snow albedo reduction, estimated by an online model – Snow, Ice, and Aerosol Radiation – was in the range of 0.8–3.8% during the pre-monsoon season. The glacier mass balance analysis suggested that BC contributed to approximately 39% of the total mass loss in the pre-monsoon season.

1. Introduction

Black carbon (BC) particles in the atmosphere originate from incomplete combustion processes. BC particles are also known as light absorbing carbonaceous particles which are primarily determined by optical methods (Petzold et al., 2013). BC particles remain in the atmosphere for several days and are removed by processes such as dry or wet deposition or by acting as a cloud condensation nuclei (Targino et al., 2009). Due to its high light-absorbing efficiency across visible and infrared wavelengths, BC has been considered as the second largest anthropogenic contributor to global warming after CO_2 (Gustafsson and Ramanathan, 2016). BC particles in the atmosphere absorbs solar radiation and can play an important role in modifying the earth's radiative

☆ This paper has been recommended for acceptance by Admir C. Targino.
* Corresponding author.
E-mail address: sivapraveen.puppala@icimod.org (S.P. Puppala).

https://doi.org/10.1016/j.envpol.2021.116544

balance (Flanner et al., 2009). Indirectly, BC particles can interact with clouds, changing their microphysical properties, and thus impacting the climate (Li et al., 2016a,b; Wang et al., 2018). The strong absorption capabilities, small size range, chemically inert nature, shorter lifetime in the atmosphere, and the predominantly anthropogenic nature of its sources make BC particles an extremely important component of climate studies (Bond et al., 2013; Zhang et al., 2020; Liu et al., 2015).

Several studies in the Himalayan region have focused on observations and the character of BC particles in the ambient air. However, though there are a large number of BC observatories in low altitudes (<2000 masl) and in the plains, only a few studies have characterized BC at high altitudes in different parts of India, China, and Nepal (Babu et al., 2011; Carrico et al., 2003; Chen et al., 2018; Ming et al., 2009; Yasunari et al., 2010). The deposition of light-absorbing aerosols on snow or ice can lead to the darkening of the surface, which would enhance the absorption of solar radiation and significantly reduce the surface albedo. Such phenomena could result in positive forcing that can accelerate snow and ice melt in high altitudes (Flanner et al., 2007; He et al., 2018; Ming et al., 2013; Zhang et al., 2015). Additionally, the acceleration in the melting of snow and ice can change the regional hydrological cycle in the mountain ranges (Qian et al., 2015). Earlier studies have suggested that the BC particles deposited on the Himalayan glaciers (snow and ice) are responsible for rapid glacier retreat (Xu et al., 2009). As such, atmospheric BC deposition over the Himalayan region and its impact on snow albedo change, resulting in rapid snow and ice melt, has been a hot topic of discussion in the research community (Gul et al., 2018; He et al., 2018; Li et al., 2016a,b, 2017). Hence, continuous measurements of atmospheric BC particles over such high-altitude locations are crucial in order to develop a profound understanding of BC and its impact on the cryosphere, which directly or indirectly affect the regional climate and the monsoon and hydrological cycle.

The glaciers in the Himalayan region, also dubbed the Third Pole, are regarded as the richest source of freshwater reserves besides the poles (Kang et al., 2019). The lives and livelihoods of millions of people residing downstream of many glacier-fed rivers in the Himalayan region are directly or indirectly affected by changes in the monsoon rainfall, river discharge, and regional climate (Dahal et al., 2019; Scott et al., 2019). Therefore, it is imperative to characterize the variability of atmospheric BC at high-altitude Himalayan areas in order to develop a better understanding of its chemistry, deposition, washout rate, and impact on albedo reduction (Niu et al., 2019).

Here, we analyse the variability of atmospheric BC mass concentration (from October 2016 to September 2017) obtained from an autonomous BC station, installed near the Yala Glacier (4900 masl) in the central Himalayan region of Nepal. The study also estimates the BC and water-insoluble organic carbon (WIOC) particles from the surface snow samples collected during the pre-monsoon season and the subsequent wet scavenging ratio during the precipitation event. It also attempts a numerical quantification of the contributions from different sources (i.e., anthropogenic, open burning) and regions (countries) to the total BC. As the final step, we estimate the surface snow albedo reduction and glacier melting in the pre-monsoon season due to BC particles.

2. Study area

The observation site (28.21°N, 85.61°E) is located near the Yala Glacier at an altitude of 4900 masl in the central Himalayan region of Nepal (Fig. 1). This autonomous BC station is currently the highest station running in the Hindu Kush Himalaya (HKH). Fig. 1 (a) gives a regional perspective of the station, 1 (b) closer view of the atmospheric BC station. It is a remote site with minimum anthropogenic activities. This region experiences four dominant seasons each year: winter (December–February), pre-monsoon (March–May), monsoon (June–September), and post-monsoon (October–November) (Marcq et al., 2010; Shea et al., 2015).

3. Methodology

3.1. Monitoring of the atmospheric BC

Continuous real-time observations of the atmospheric BC mass concentrations were made using an aethalometer (AE 33, Magee Scientific, USA). The equipment was operated at a constant flow rate of 2 L min^{-1} and sampling rate of 1 min. It was generating 1 min temporal resolution data, but we averaged it for 10 min resolution to avoid any noise due to low concentrations. This flow rate was periodically checked with a high-quality bubble meter (Mini-Buck Calibrator M-5, A.P. Buck Inc., Orlando, USA) that matched 99.6% with the recordings of the aethalometer. The sampling inlet was fitted with a $PM_{2.5}$ (particulate matter with aerodynamic diameter < 2.5 μm) cyclone. The inherent uncertainties (viz. multiple scattering and shadowing effects) associated with the use of a filter-based optical attenuation measurement technique were processed by the means of in-built algorithms in the aethalometer (Drinovec et al., 2015). Hence, the values obtained from the aethalometer at 880 nm were used directly without applying any further corrections. BC particles absorb at 880 nm for both fossil fuel and biomass generated sources. The spectral dependence of absorption towards lower wavelength (UV region) for fossil fuel is weak compared to biomass sources which means BC particles from biomass burning have stronger absorption in the ultraviolet region than fossil fuel, which absorbs mostly in the infrared (Kirchstetter et al., 2004; Krecl et al., 2020).

3.2. Meteorological measurements

Meteorological parameters such as temperature, radiation, wind speed, humidity, wind direction, and precipitation were measured using sensors appropriate for high-altitude measurement. Wind speed and wind direction were measured using a Wind Monitor-Alpine (Model 05103-45; Young, USA). A WS301-UMB Smart Weather Sensor (LUFFT, Germany) was used for measuring relative humidity, temperature, pressure and solar radiation. A Pluvio2 (OTT, USA) sensor was used to measure the intensity and amount of precipitation in liquid and solid forms. All sensors were installed as per the World Meteorological Organization (WMO) guidelines. They were factory calibrated and installed near the observation site for the very first time for our research.

3.3. Sampling and analysis of BC and WIOC in surface snow

Snow samples were collected from near the observation site during the summer campaign to estimate the concentration of BC and WIOC. Before the commencement of snow sampling on May 1, 2017, there was fresh snowfall around the study site. The mean snow thickness of fresh snow was around 15–18 cm and we collected samples from the top 7–10 cm layer. Six samples (out of 22) were collected from the nearby sites of the observatory on 1 May during snowfall time, and were considered mostly fresh samples. These six samples were collected during precipitation events at six different timings and locations near the study site. On the following days (2–3 May 2017), 14 more samples were collected from the surface of the Yala Glacier. Two samples were collected near the section where the Yala glacier ends. All snow samples were collected at a minimum separation distance of 50 m during or after

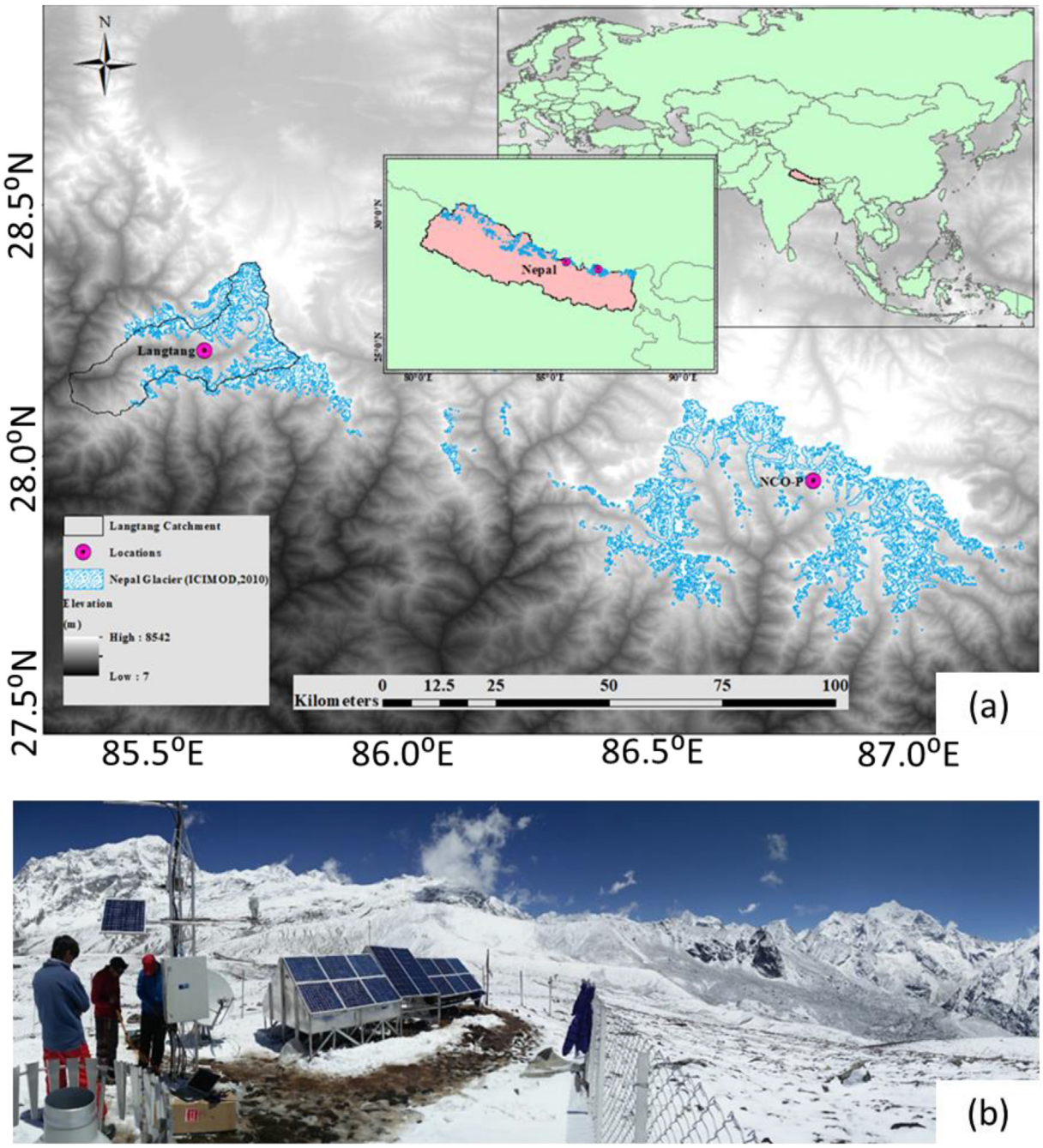

Fig. 1. The study area map showing the autonomous atmospheric BC station and NCO−P marked by pink circles. The below portion is a closer view of the atmospheric BC station. (For interpretation of the references to color in this figure legend, the reader is referred to the Web version of this article.)

the snowfall events.

The samples were collected and analysed according to the procedure given in Gul et al. (2018); Li et al. (2017); Niu et al. (2020); Zhang et al. (2017). Snow density, snow grain size and snow thickness were estimated for each sample through a small density kit, snow card and numbers scale respectively. In a temporary laboratory near the sampling site, the snow samples were melted and immediately filtered using pre-combusted (550 °C, 6 h) quartz fibre filters of 47 mm diameter (QM/A, Whatman, UK) and a vacuum pump (Gul et al., 2018; Li et al., 2018; Zhang et al., 2018, 2017). There also exist limitation of proper filtration of BC particles associated with quartz fibre filtration process (Cereceda-Balic et al., 2019) that might lead to certain amount of underestimation and hence results should be used with caution. Although earlier studies also indicate that the BC collection efficiency of the filtration of melted snow samples was determined to be 77 ± 17% (Li et al., 2016a,b). After filtering, the filter papers were placed in a petrislide, sealed by Teflon tape and kept in powder-free clean plastic zip lock bags. They were properly labelled and stored at −20 °C until further analysis. Two blank quartz filters were also collected simultaneously in order to eliminate any possibility of contamination in the collection media and/or influences due to the transport and handling of the filter samples. The sample filters and blanks were then transported to the State Key Laboratory of

Cryospheric Sciences (SKLC), Northwest Institute of Eco-Environment and Resources (NIEER), in Lanzhou, China, for the analysis of BC and WIOC using the thermal optical (filter-based) analysis method, described in (Zhang et al., 2017, 2018). The thermal/optical measurement method identified the analytical results as elemental carbon (EC) and organic carbon (OC). As the dust loads in the snow samples were greater than those in the airborne aerosol samples, the method was modified such that, in a 100% helium atmosphere, only one temperature plateau (550 °C) was used to reduce the time that the BC was exposed to the catalysing atmosphere. The carbon analyzer can effectively measure between 0.1 and 4000 μg carbon/cm^2 for a typical punch size of 0.5 cm^2. To identify uncertainty stemming from instrumental instability and the uneven distribution of carbon particles in the filters, duplicates of ~25% of the samples were analysed separately. More details of calibration procedure have been provided in the supplementary material S1. The mean mass concentration of BC and WIOC for both the blank filters was 0.01 ng g^{-1} and 0.02 ng g^{-1}, respectively. The final mass concentration of BC and WIOC was measured by subtracting the mean value of the field blanks from the mean BC and WIOC concentration measured in the sample quartz filters.

3.4. Source studies using absorption Ångström Exponent (AAE) (in situ measurements)

Frequently, AAE values for fossil fuel and biomass burning sources are calculated at 470 and 950 nm wavelengths ($AAE_{(470/950)}$) which is an indicator of spectral dependence of absorption and also provides source information. Past studies had narrowed down the AAE of fossil fuel sources from 0.5 to 1.1, while a broader range of 0.9–3.5 was observed for biomass-burning sources based on different particle sizes and flaming conditions (Kirchstetter et al., 2004; Liu et al., 2016, 2018; Romonosky et al., 2019), more details have been explained in S9(a). The aethalometer (AE-33) used in the present study determined the biomass/fossil fuel contribution to BC by making use of an internal algorithm that assumes $AAE_{(470/950)}$ values 1 and 2 for fossil fuel and biomass-burning sources, respectively (Drinovec et al., 2015). These values might not be able to present the variability arising with respect to changes in biomass type and combustion processes associated with the burning events and transport of aerosols. Thus might not indicate the actual representation of the aerosols observed at the study site. Moreover, most of the time, the aerosols reaching high altitude sites in central Himalayas (in this case the study site) are one–three days old (Putero et al., 2014, 2018) and go through transformation due to the extreme metrological conditions. Thus, it is difficult to exactly define the AAE for biomass and fossil fuel sources as they could be transported aerosols or freshly emitted ones from different combustion processes, leading to uncertainties in the calculation of the contributions (supplementary material S9(b)). Past field and laboratory based research on AAE values also present a wide range of variability (Kirchstetter et al., 2004; Krecl et al., 2020; Liu et al., 2016, 2019; Romonosky et al., 2019). Therefore, in the present study the $AAE_{(470/950)}$ values of 1.68 and 0.9 for biomass and fossil fuel sources, respectively, recommended by Zotter et al. (2017), were considered for aerosols fresh conditions. The $AAE_{(470/950)}$ values of 1.2 and 0.5 for biomass and fossil fuel, respectively, were assumed for aerosols aged conditions (Liu et al., 2016; Romonosky et al., 2019). For both the cases above, the $AAE_{(470/950)}$ values greater than equal to the upper limit (1.68/1.2) indicate 100 percent biomass whereas less than or equal to the lower limit (0.9/0.5) indicate 100 percent fossil fuel. In between we derive the biomass and fossil fuel contribution using methodology given by Sandradewi et al. (2008). Since atmospheric BC measurements were reported for 880 nm wavelength, we interpolated the source contribution results for 880 nm using the equation below (equation (1)) to maintain consistency of reporting. More details about the in situ measurements, the spectral dependence of aerosol absorption at different wavelengths, and its limitations can be found in the supplementary material S9(a).

$$\frac{T_\lambda}{T_{\lambda 0}} = \left(\frac{\lambda}{\lambda 0}\right)^{-\alpha} \quad (1)$$

where, T_λ is the optical thickness at wavelength λ, $T_{\lambda 0}$ is the optical thickness at wavelength λ0 and α is the Ångström Exponent.

3.5. Scavenging ratio

Based on simultaneous measurements of the atmospheric BC, the BC in the surface snow samples, and the precipitation event during the snow-sampling time, we calculated, using equation (2), the scavenging ratio of the BC particles in order to understand the efficiency of BC scavenging by precipitation:

$$\text{Scavenging ratio} = \frac{BC\ concentration\ in\ snow\ sample}{Atmospheric\ BC\ concentration} * \rho \quad (2)$$

ρ is the density of air, which was approximately 0.719 kg m^{-3}, and was corrected using local pressure and temperature before implying it for the calculations of the present study. In this study, the scavenging ratio was calculated for only six fresh snow samples (n = 6), which were collected during a single precipitation event near the observation site. Although the units of the BC in snow and air were ng g^{-1} and μg m^{-3}, respectively, for these specific calculations, we converted the BC in snow values from ng g^{-1} to μg m^{-3}, thereby making the units the same for both the values. We calculated the hourly mean concentration of atmospheric BC and estimated the BC in surface snow during the precipitation event. We did this comparison for just one day when there was snowfall during the snow-sampling time (n = 6). Simultaneous measurements of the BC particles in air/precipitation have been carried out by several authors in the past to estimate their scavenging ratio (Armalis, 1999; Granat et al., 2010; Hegg et al., 2011). This approach of measuring BC from atmosphere and surface snow, however, has some limitations which have been discussed in a separate section (see supplementary material S1 a,b).

3.6. Surface snow albedo

The surface snow albedo during the pre-monsoon season was estimated using an online model called SNICAR (Snow, Ice, and Aerosol Radiation) (Flanner et al., 2007). The BC mass concentration estimated from the snow sample analysis was fed as input into the model. Other parameters such as the environment, snow density, and grain size (measured in the field) were also given as inputs to the model. The snow density was estimated in situ via a small snow-density kit during the snow-sampling time period. The size of the snow grain (~120 μm) was estimated with the help of a snow card. Table 1 shows these input parameters.

3.7. Modeling snow/glacier mass loss

We used a mass-balance model with energy balance approach to estimate the snow/ice mass loss (Hock and Holmgren, 2005; Kayastha et al., 1999; Reijmer and Hock, 2008). The net energy available for the melting of snow/ice (Q_M) is the sum of the net shortwave radiation (S_{net}), net longwave radiation (L_{net}), sensible heat flux (Q_H), latent heat flux (Q_L), heat conduction flux (Q_G) and energy flux from rain (Q_P). More details about the model are given

Table 1
Concentration of BC and WIOC in the collected surface snow samples from the Yala Glacier during May 2017. The values in columns 1 and 2 have been rounded off to the nearest whole number. SZA refers to Solar Zenith Angle.

S/N	BC (ng g^{-1})	WIOC (ng g^{-1})	Ratio (WIOC/BC)	SZA	% albedo reduction via model	Snow grain size (μm)	Snow density (kg m^{-3})	Snow thickness (m)
1	196	260	1.3	31	1.5	118	80	0.05
2	175	207	1.2	37	1.3	118	75	0.05
3	105	152	1.4	43	0.8	116	76	0.05
4	193	266	1.4	49	1.3	119	92	0.05
5	249	512	2.1	56	1.5	119	72	0.05
6	320	793	2.5	60	1.8	116	85	0.05
7	303	653	2.2	52	1.9	117	217	0.05
8	175	376	2.1	40	1.3	123	225	0.05
9	303	653	2.2	33	2.2	125	218	0.05
10	382	750	2.0	21	2.9	129	229	0.05
11	206	336	1.6	15	1.7	122	216	0.05
12	205	323	1.6	62	1.2	126	234	0.05
13	449	563	1.3	56	2.6	129	220	0.05
14	204	240	1.2	45	1.4	130	229	0.05
15	275	563	2.0	39	1.9	124	234	0.05
16	382	609	1.6	30	2.7	133	250	0.05
17	542	827	1.5	23	3.8	123	239	0.05
18	322	630	2.0	15	2.5	122	265	0.05
19	249	439	1.8	12	2.0	127	254	0.05
20	145	449	3.1	16	1.2	124	242	0.05
21	189	302	1.6	22	1.5	128	238	0.05
22	96	212	2.2	26	0.8	132	245	0.05

in supplementary material S2. We used observed meteorological data and surface conditions such as snow density and roughness parameters from the Yala glacier as input to simulate the model (Acharya and Kayastha, 2018). Surface albedo is a critical aspect in the model, directly affecting the net shortwave radiation and ultimately net energy available for mass loss. The impurities (such as atmospheric BC) deposited over snow/glacier surface alters the albedo thus affecting the melting process/mass balance. Hence, to understand the BC impact on glacier mass balance, we simulated the model with three albedo values representing no BC, observed BC and biomass BC fraction (calculated in section 4.4) in snow/ice. For these three scenarios, all other parameters and meteorological parameters were kept constant. The albedo changes were calculated using SNICAR model, version 2 (Flanner et al., 2007; He et al., 2018). Notably, the calculations under scenarios two and three were carried out only during the pre-monsoon season as snow/ice BC data was not available for other seasons. Earlier, same model was applied and validated over the Yala glacier by (Acharya and Kayastha, 2018). Apart from that, a similar approach was used globally at different locations i.e. Indian Himalayas, Washington (USA), Bolivia, Antarctica, Chile, Norway, Alaska (USA), Tibetan Plateau, French Alps, and northern Sweden for the energy balance modeling of glaciers (Anslow et al., 2008; Azam et al., 2014; Braun and Hock, 2004; Giesen et al., 2014; Klok et al., 2005; Pellicciotti et al., 2008; Sicart et al., 2008, 2011; Zhang et al., 2013).

3.8. Chemical transport model: potential source regions and source contributions

The weather research and forecasting model, coupled with chemistry (WRF-Chem) simulations (Grell et al., 2005), was used to identify the potential source regions of the atmospheric BC particles arriving at the observation site. This model uses region-tagged atmospheric BC tracers for different regions across the world in order to identify the geographical emission sources (Kumar et al., 2015). It has also been used in other chemical transport models (He et al., 2014a; Ikeda et al., 2017). We archived the model results on an hourly basis – from 00 UTC on September 1, 2016 to 23 UTC on August 31, 2017 – thereby covering a whole one-year period. The spatial resolution of the model was 20 km × 20 km, with 35 vertical levels stretching from the surface up to 50 hPa (~20 km). The applied WRF-Chem model version was 3.9.1.1, and it used the Fire Inventory from NCAR (FINN) for biomass emissions, the EDGAR-HTAP for anthropogenic emissions, and MEGAN (Model of Emissions of Gases and Aerosols from Nature) for the biogenic emissions calculated online. The FINN emission was prepared to exactly match the simulation time (2016–2017). MEGAN is an online calculation model, and the time period exactly matches the simulation period. The EDGAR-HTAP project compiled a global emission data set with annual inventories for CH_4, NMVOC, CO, SO_2, NOx, NH_3, PM_{10}, $PM_{2.5}$, BC, and OC, covering the period of 2010. The Model for OZone And Related Chemical Tracers (MOZART) was applied for the gas-phase chemistry (Knote et al., 2014), while the aerosols in the WRF-Chem were simulated via the Model for Simulating Aerosol Interactions and Chemistry (MOSAIC) (Zaveri et al., 2008). The other model components and set-up have been described in detail by Kumar et al. (2015). We used the Global Data Assimilation System (GDAS) from the National Center for Environmental Prediction (NCEP) for the meteorological boundary condition. The aim of the model simulation was to quantify the impact of anthropogenic and open-burning emissions, estimate the BC concentration in the atmosphere, and to identify the geographic source regions contributing to the observed atmospheric BC at the field sites (Region 1 China, 2 Nepal, 3 India, 4 Pakistan, 5 Afghanistan, 6 Bhutan, 7 Bangladesh, 8 Myanmar, 9 Southeast Asia, and 10 rest of the region). Due to gridding issues that existed in the border regions of Nepal and India, it was not possible to completely segregate the emissions in order to determine whether they were from Nepal or India; hence, the emissions from these two regions were clubbed together in the analysis. The simulations provide data on the total atmospheric BC, the atmospheric BC generated by open burning (forest fires and open agricultural burning detected by satellites), anthropogenic atmospheric BC (represents transport, industry, household energy, garbage etc.), and boundary atmospheric BC, thus enabling us to quantify the contribution from each of these sources (open-burning sources, anthropogenic sources, and the atmospheric BC coming from the boundary conditions). The actual biomass sources could be forest fires, large scale open burning and household energy using solid fuel (cooking and heating) and biomass garbage fires etc. Thus part of biomass was

considered anthropogenic in WRF-Chem simulations as a result of which this simulation cannot clearly define biomass and fossil fuel sources; rather it only differentiates open burning and anthropogenic sources. Apart from that, biogenic emissions might result in formation of certain secondary organic aerosols (Guenther et al., 2012) which will not influence the BC sources. Hence, in this simulation we only discuss biomass vs anthropogenic sources but not biogenic sources. To have a better understanding of the biomass burning and fossil fuel source contribution, we use AAE based calculations given in section 3.4. As the effect of the boundary conditions was minimal, this was not discussed further. Although the model runs exert a significant impact on the study, there remain a few limitations to it (see supplementary material S3).

4. Results and discussions

4.1. Meteorological variations

The mean temperatures at the study site were recorded −6.6 °C in winter, −4.3 °C in pre-monsoon, 2.6 °C in monsoon, and −1.6 °C post-monsoon, and these were similar to the observations made in a nearby region (Yasunari et al., 2013). The predominant wind direction (south-west) was up-valley and the mean ± standard deviation wind speed during the observation period was 2.1 ± 1.6 m s^{-1}. The wind rose plots discussed earlier in Rai et al. (2019) indicated higher frequency of winds arriving at the observation site from the south-western direction, followed by the north-eastern sector, thus representing a bimodal distribution. The winds arriving from the south-western direction would bring in air mass from the polluted Indo Gangetic Plain in the south, while the north-eastern part would bring in certain amount of pollutants from the Chinese mainland. Our results indicate that the beginning of the monsoon is in June, with most of the precipitation occurring in July, August, and September. Prior research at the NCO—P (Nepal Climate Observatory-Pyramid, located 122 km east of our sampling site), had also yielded similar findings for the monsoon season (June—September) (Marinoni et al., 2010). A more detailed description of the meteorological conditions and their effect on BC is provided in Rai et al. (2019). The temporal variations in the different meteorological parameters during the study period are shown in supplementary material S4.

4.2. Temporal variability in in situ and model-simulated atmospheric BC mass concentration

The time series of in situ atmospheric BC observations (October 2016 to September 2017) and that derived from the WRF-Chem model simulations (September 2016 to August 2017) are shown in Fig. 2. The annual mean ± standard deviation of atmospheric BC mass concentration observed from in situ observations was 0.42 ± 0.57 μg m^{-3} and that from the model simulations was 0.73 ± 0.51 μg m^{-3}, thereby indicating an overestimation in terms of the modelled data sets. Seasonally, the atmospheric BC mass concentration, observed in situ, reached its maximum during the pre-monsoon season (0.73 μg m^{-3}), followed by winter (0.46 μg m^{-3}), and post-monsoon (0.29 μg m^{-3}), while it was at its minimum during the monsoon (0.23 μg m^{-3}). Similar seasonal variability was also observed in the modelled data sets but with a higher magnitude (see Fig. 2a and supplementary material S5). A close similarity was also observed between the seasonal variability of the atmospheric BC obtained from the in situ data and those from the nearby regions (S5) (Babu et al., 2011; Chaubey et al., 2012; Chen et al., 2018; Marinoni et al., 2013; Nair et al., 2013; Ram et al., 2008, 2010). A correlation plot between the daily mean atmospheric BC obtained from model simulations and in situ observations (r^2 = 0.32) (supplementary material S6) indicated a weak positive relation. The WRF-Chem simulations with a spatial resolution of 20 km may not be adequate to capture the complex terrain of the Himalayan region (described in detail in supplementary material S3). Aside from these limitations of modelled atmospheric BC over the high-altitude Himalayan region, the estimates in the present study are at least capable of capturing the variability. Thus, in order to improve the model-based results, it is important to have high-resolution model simulations in order to improve the BC simulations in the Himalayas and the surrounding regions. In addition to the model resolution issue, some key model physics and parameterizations in the WRF may also have inflected our modeling analysis with uncertainties. For example, recent studies He et al. (2019) and Liu et al. (2019) have suggested that the WRF simulations tend to overestimate the snow cover over complex mountain terrains − even at a 4-km high resolution − due to model parameterization biases, which further leads to a cold bias in reading the surface temperature. These uncertainties in the meteorological field may, in turn, affect atmospheric BC simulations when it comes to transport and deposition. However, a full exploration of the potential uncertainties associated with each of the key model physics requires further substantial efforts which lie beyond the scope of the present study.

In order to analyse the impact of forest fires on BC evolution at the study site, a plot of the fire counts during the entire study period over the plains south of the study site has been shown in Fig. 2 (b). As evident from the figure, the peaks in atmospheric BC mass concentration closely match the peak in fire counts in the month of April. The mean atmospheric BC mass concentrations in the month of April are approximately 2.5 times higher than the annual mean, indicating that the highest concentration of atmospheric BC occurs during this month. The multiple episodes of high concentrations of atmospheric BC (above 4 μg m^{-3}; see supplementary material S7) during the pre-monsoon season can be attributed to the increase in open-burning events in the adjacent plains (viz. the Indo-Gangetic Plains), coupled with long-range transport of pollutants from these regions to the study site/the Himalayas. Studies in the past have also suggested how the convective lifting of pollutants and their subsequent transport through the trans-Himalayan valleys during the pre-monsoon season provide a significant opportunity for the pollutants to be transported high up into the mountains (Bonasoni et al., 2010; Dhungel et al., 2018).

In the present study, a distinct diurnal cycle, typical of high-altitude locations, was observable, with the lowest atmospheric BC concentration being in the night-time, followed by a gradual increase after sunrise and reaching its peak during early to late afternoon depending on the season. This variation was most pronounced in the pre-monsoon season, with peaks during 13:00—17:00 h local time, whereas in other seasons, the peaks were visible just before noon till evening. The supplementary material S8 shows this diurnal variation in the atmospheric BC through in situ observations and model simulations for the four seasons. Similar diurnal variations with shifts in peak hours have also been reported in previous research conducted in different high-altitude locations in India, Nepal, China, and the European Alps (Babu et al., 2011; Baltensperger et al., 1997; Chen et al., 2018; Marinoni et al., 2010). The diurnal variations depicted by the model simulations did not follow a fixed pattern unlike in the case of in situ observations, indicating the biases that model simulations can inherit in the Himalayan region as discussed above.

4.3. Concentrations of BC and WIOC in surface snow

The mean ± standard deviation BC and WIOC concentrations

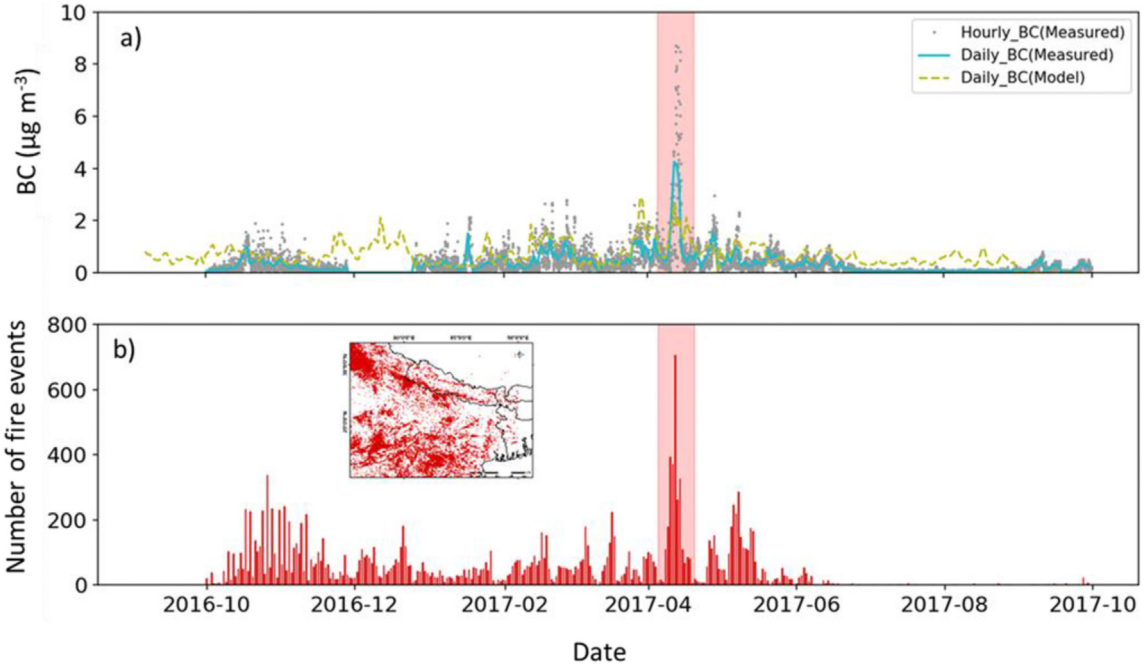

Fig. 2. (a) The time series of atmospheric BC for a period of one year observed at the autonomous atmospheric BC station and that derived from the model for the observation site; and (b) the daily MODIS-derived open-burning counts during the study period. The red patch in each panel highlights peak fire events in the month of April 2017. (For interpretation of the references to color in this figure legend, the reader is referred to the Web version of this article.)

during the campaign period were estimated to be 257 ± 111 ng g^{-1} and 460 ± 206 ng g^{-1}, respectively (Table 1). A strong correlation between BC and WIOC ($r^2 = 0.7$) indicates similarity in source. As the campaign period coincided with the pre-monsoon season, the sources of BC/WIOC could be attributed to the transport of air masses from the plains situated to the south of the observation site where open burning is a prominent phenomenon. To further ascertain the source of these emissions, we calculated the WIOC to BC ratio. Research has suggested a wide range of variability in the OC/BC ratio by taking into consideration different locations such as plains, oceans, and urban and rural areas, as outlined in a study by Bond et al. (2004). Another study by Gul et al. (2018) has indicated a variation in OC/BC – from 0.04 to 4.88 – in different glaciers of Pakistan but at a much lower elevation. Generally, a lower WIOC/BC ratio is linked to fossil fuel sources, while a higher ratio is linked to biomass-burning sources (Zhang et al., 2017, 2019). Throughout the sampling period, the WIOC/BC ratio in individual snow samples ranged between 1.2 and 3.1 (with a mean of ~2) that might not exactly be able to point out a particular source. However, due to more number of fire spots observed during this season (Fig. 2b) (Putero et al., 2014), a higher biomass fraction can be expected. Simultaneous increase in the atmospheric BC was also observed during the same period. Hence, the inference is that the WIOC/BC ratio observed in this study can be indicative of biomass-burning source. There are also a few uncertainties in the analysis of WIOC/BC, starting from sample collection, including the method used for the analysis, the amount of dust loading on the sample, and the presence of metal oxides and calcium carbonate. These uncertainties have been widely discussed in the past (Ahmed et al., 2009; Blanco-Alegre et al., 2019; Cereceda-Balic et al., 2019; Lack et al., 2014; Schwarz et al., 2012; Wendl et al., 2014) and can be found in supplementary material S1b. The literature indicates that the OC/BC ratio can be altered in the presence of metal oxides either by enhancing OC charring or by lowering the BC oxidation temperature (Wang et al., 2010); this can also interfere with the thermal optical protocols (Wu et al., 2016). However, in a region beset by severe data limitations, even a few observations, as in this present study, can be valuable to the scientific community since they help build the scope for further research caution should also be applied while interpreting the results.

4.4. Source apportionment

4.4.1. In situ measurement-based estimation

Considering the case of fresh ambient conditions, the contribution of biomass burning to the atmospheric BC mass was estimated to be ~54%, 44%, and 45% at 470-nm, 880-nm, and 950-nm wavelengths, respectively, for the entire study period. In the case of aged ambient aerosols, the biomass-burning contribution to the total atmospheric BC mass during the entire study period was approximately 82%, 80%, and 78% at 470-nm, 880-nm, and 950-nm wavelengths, respectively. Using only the 880-nm wavelength, we tried to understand the seasonal contributions of the different sources in the case of “fresh ambient conditions” and “aged ambient aerosols”. The seasonal distribution of source contribution was considered as a spectral dependence of aerosol absorption at different wavelengths which were observed to be better when visualized seasonally (more details explained in S9). In the case of fresh ambient conditions, the biomass-burning fraction was ~46–47% during all the seasons barring the monsoon when it went down to 34%. However, for the month of April, the biomass contribution rose to approximately 49%. As regards the aged ambient condition, the biomass-burning fraction was ~77% for post-monsoon, 81% for winter, 87% for pre-monsoon, and 69% for monsoon. Notably, for the month of April, the biomass-burning contribution rose to approximately 90%, thus indicating that during this month, there is a stronger contribution of biomass-burning aerosols transported in significant quantities from the plains south of the study site. It has to be also stated that, in the present case, an exact quantification of the biomass-burning source or fossil fuel

source contribution was not possible due to certain limitations (as discussed in detail in supplementary paper S9). However, this calculation would provide the limits of variability in the biomass-fraction contribution at different wavelengths and under different conditions that are affecting the study site. Moreover, the contributions from the fresh ambient conditions would be more representative as the aged conditions could exaggerate the biomass contribution.

4.4.2. WRF-Chem model-based calculation

Model results indicate that throughout the year, anthropogenic sources strongly dominated (77%) the atmospheric BC mass near the Yala Glacier region, followed by open-burning sources (14%). However, when the seasonal picture was considered, anthropogenic sources contributed 55–97% during the different seasons, while open-burning sources contributed less than 1–~28% during the different seasons. Importantly, it was observed that the contribution from the open-burning sources near the Yala Glacier region was the highest during the pre-monsoon season (~28%), with the peak contribution in the month of April (~34%) as shown in Table S3. This closely matched the peaks in atmospheric BC concentrations at the observation site and the occurrence of forest fires in the low-lying region south of the study site, thus corroborating the strong effect of long-range transported aerosols reaching the observation site, particularly in the month of April. Moreover, the anthropogenic sources simulated by the WRF-Chem model included certain amount of biomass-burning emissions as well as fossil fuel emissions, hence open burning would not represent the total atmospheric BC from all the biomass-burning sources. Therefore, the picture of the contribution of biomass burning as discussed in the section above (4.4.1) could be considered as a representative one.

4.5. Regional contribution using the WRF-Chem model

We show the regional contribution of BC from the surrounding countries during September 2016 to August 2017 in Fig. 3. The results shown in Fig. 3 are the anthropogenic atmospheric BC source contribution of each region to the surface atmospheric BC out of the total anthropogenic sources within the study domain (the details are given in supplementary material S10). The highest contribution of atmospheric BC was from Nepal and India combined during the entire study period. Annually, the atmospheric BC contribution from Nepal and India combined was approximately 69% (64–74% depending on the season), followed by 22% from China, 3% from Bangladesh, 2% from Pakistan, 1% from Bhutan, and the rest from the nearby regions. Though the contribution varied slightly from season to season, India and Nepal together, followed by China, were the major contributors of atmospheric BC at the Yala Glacier throughout the year. Although the region presented in our study falls under the influence of the westerlies and the Indian monsoon, still a high contribution is observed from China. This is mainly due to the proximity of the study site to the Chinese border (~3 km). There are three Chinese cities near this site, namely Gyirong, Naylam, and Zhangmu. Thus, a large portion of the Chinese contribution could come from local emissions in the Tibetan Plateau and the Himalayan regions. Research of Marinoni et al. (2010) at the NCO–P (5079 masl) also indicates that certain amount of pollution can be attributed to transport from the nearby Tibetan Plateau. An earlier study by Rai et al. (2019) also indicates that there is some contribution of atmospheric BC mass from the north-east sector (representing emissions from the nearby regions in the north, i.e. China) although a major contribution is from the south-west sector. In addition, He et al. (2014b), using a global chemical transport model with tagged BC tracers, showed that the BC over the Himalayan and central Tibetan regions is mainly contributed by emissions in South Asia (~60%) across the year, with ~10–20% contribution from China, while ~20–30% of all the rest of the emissions are carried by the westerlies and other long-range transport to the region. Zhang et al. (2015) adopted a similar BC-tagging method in a global climate-chemistry model and found that, in the Himalayas and the central Tibetan Plateau, BC emissions from South Asia had the largest contribution (50–90%) depending on the season, with ~10% from local emissions in the Himalayas and the Tibetan Plateau (HTP) and another ~10% contribution from China's regions outside the HTP. The rest of the sources (including pollution transported by the westerlies) generally showed a small overall contribution (~10–20%). Thus, the source contribution results from this study are generally consistent with those of previous studies.

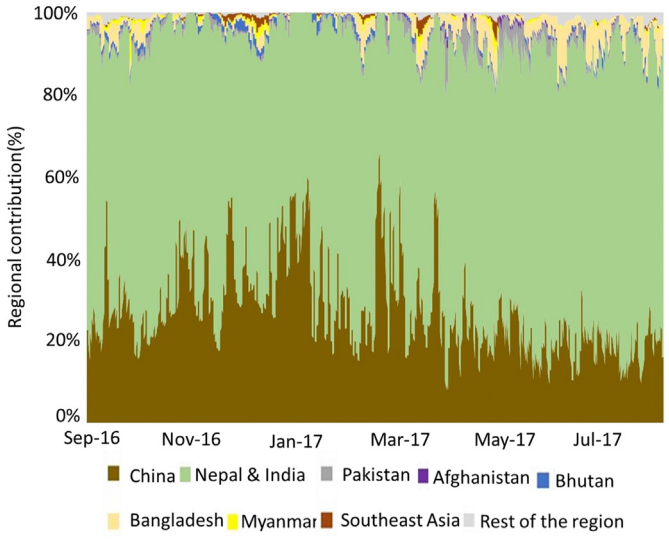

Fig. 3. The potential source region attributions of the atmospheric BC identified by the WRF-Chem model simulation from September 2016 to August 2017, which is the anthropogenic BC source contribution of each region to the surface BC out of the total anthropogenic sources within the study domain.

4.6. Scavenging ratio estimates

The atmospheric BC mass concentration and BC concentration in snow and its corresponding scavenging ratio in the case of six fresh snow samples collected during a single precipitation event are shown in Table 2. The scavenging ratio during the snow-sample collection ranged from ~140 to 466. The mean ± standard deviation atmospheric BC during the time of collecting the six snow samples was 530 ± 181 μg m^{-3}, while the simultaneous BC in the snow samples was 305 ± 125 ng g^{-1}, and the scavenging ratio 206 ± 72, which indicates a wide variability in the scavenging ratio. The results obtained from this analysis are from a small sample size that might not be representative of an entire season. This scavenging ratio can significantly change when it comes to long-term observations of precipitation events, as the precipitation rates and the duration of the events would differ. There may exist certain limitations in estimating the BC mass concentration due to the different techniques used to measure the ambient air and snow samples and also due to the small sample size. However, this was the best possible data set that could be obtained considering the geographical location of the site, the adverse conditions faced by the researchers, and the available estimation procedures. The overall limitations of this study and the importance of the data sets

Table 2
The scavenging ratio estimated from the BC in air and snow near the observation site and in comparison with other sites. The values in columns 2, 3, and 4 have been rounded off to the nearest whole number.

May 01, 2017	Avg. precipitation (mm hr^{-1})	BC in atm. (μg m^{-3})	BC in snow (ng g^{-1})	Scavenging ratio (SR)	Remarks
13:45	1.2	303	196	466	Present study
14:15	0.5	311	175	404	Present study
14:42	0.4	541	105	140	Present study
15:11	0.2	704	193	197	Present study
15:40	0.2	662	249	271	Present study
15:56	0.1	657	320	350	Present study
Time Period	**Location/Analysis methods**			**(SR)**	**Reference**
10-year mean	Three-dimensional global model estimate of worldwide mean[a]. The mass-scavenging ratio of BC due to snowfall was the mass mixing ratio of BC in snowmelt divided by BC in air.			125	Jacobson (2004)
Spring 2007	Svalbard archipelago (78.917°N, 11.933°E): Zeppelin Observatory (475 masl) and the Sverdrup research station in Ny-Ålesund (8 masl)/BC in fresh snow and in air was measured by multiwavelength spectrophotometer and Particle Soot Absorption Photometer respectively.			April: 554 ± 81 May: 1057 ± 270	Hegg et al. (2011)
Spring 1984	4 sites in Abisko, Sweden/Filter based optical analysis method. Quartz fiber and nuclepore filters were used for the determination of the atmospheric BC and BC in snow respectively, and were analysed by optical analysis method. Washout ratio for BC was calculated by comparing the air and snow concentrations of BC.			101.2 ± 52.8 (54–191) mean	Noone and Clarke (1988)
May 2005 to February 2007	Maldives Climate Observatory, Hanimaadhoo/Soot in rainwater were determined on the filter with a soot photometer, and Particle Soot Absorption Photometer was used to measure it in air.			500-Trajectory 1 190-Trajectory 2	Granat et al. (2010)

[a] Three-dimensional global model is a model in which time-dependent spectral albedos and emissivities over snow and sea ice were predicted with a radiative transfer solution, rather than prescribed, was applied to study the climate response of fossil fuel plus biofuel black carbon plus organic matter when BC absorption in snow and sea ice was accounted for. The model treated the cycling of size-resolved BC + organic matter between emission and removal by dry deposition and precipitation from first principles.

have been described in the supplementary material S1a,b. Caution should also be applied while using these dataset. Compared to the study at Svalbard archipelago (April: 554 ± 81; May: 1057 ± 270, the mean of four sites) and the Maldives Climate Observatory at Hanimaadhoo (190–500), our study showed a lower scavenging ratio. However, compared to the Arctic region (98 ± 46; 101.2 ± 52.8), the ratio was slightly higher. Moreover, compared to the worldwide mean scavenging ratio of 125, simulated from global model (Jacobson, 2004) over a decade, our results were moderately higher. This indicates the necessity of estimating such ratios both at the local and regional levels. This also emphasizes the importance of long-term observations in order to improve the observation methodology and overall model estimates and also to better understand the local scenario.

4.7. Estimation of snow albedo reduction

The modelled (SNICAR simulated) snow albedo reduction only due to BC was estimated to be in the range of 0.8–3.8% during the pre-monsoon season. Table 1 (last column) gives the albedo reduction estimated via the SNICAR model from individual samples (figure shown in supplementary material S11). The results obtained from the present study were observed to be in range with previous studies performed in the region. For example, Yasunari et al. (2010) estimated the surface snow albedo reduction at the NCO–P site to be in the range of 2–5.2% during the pre-monsoon season. A study by Nair et al. (2013) indicated a surface snow albedo reduction by 1.5–4.6% over the southern slopes of the western trans-Himalayas. The WRF-Chem model, coupled with SNICAR, simulated over High Mountain Asia by Sarangi et al. (2019) indicated a snow albedo reduction in the range of 4%–8% in the pre-monsoon season, while another model-based study by Santra et al. (2019) performed over the Hindu Kush Himalayan region indicated a snow albedo reduction of 4–18%. However, this season is also associated with frequent precipitation events that lead to the mixing of BC with fresh snow. Hence, the albedo reduction estimated during this time period might be less than that in the non-precipitation periods. During non-precipitation periods, the BC might accumulate due to sublimation and dry deposition from the ambient air; hence, the albedo reduction might be even higher in comparison with the precipitation periods.

4.8. Estimating the impact of BC on glacier mass loss

Based on our simulation for scenario 1, which represent BC free snow/ice, the albedo was found in the range of 0.78–0.81 during different season, highest in the winter and lowest in the monsoon seasons. For this scenario, the highest mass loss was seen in the post-monsoon season (−5.35 kg m^{-2} per day), followed by the monsoon (−3.86 kg m^{-2} per day), and pre-monsoon (−2.50 kg m^{-2} per day), while the gain in mass was observed during the winters (3.02 kg m^{-2} per day). This variability could be attributed to the prevailing meteorological conditions, primarily the temperature and precipitation. Earlier, field-based observations at Yala glacier revealed the annual mass loss at the rate of - 4.74 kg m^{-2} per day, which is higher than our estimation of −2.17 kg m^{-2} per day (considering clean ice/snow conditions) during the same period (Acharya and Kayastha, 2018). In the second scenario, we found a 5.06% reduction (0.75) in the albedo due to the observed BC in snow/ice in the pre-monsoon season. The albedo 0.75 contributed to a mass loss at the rate of 3.47 kg m^{-2} per day in the pre-monsoon season. Which is approximately 39% higher than the mass loss due to BC free snow/ice conditions. In this study BC induced ablation was observed to be 0.97 kg m^{-2} per day. A study by Ginot et al. (2014) has estimated a mean melt rate of 1.19 kg m^{-2} per day due to BC at the Mera Glacier in the inter-monsoon season (1999–2010). The Mera Glacier (27°43′ N, 86°53′ E, area 5.1 km^2) is located on the southern slope of the Himalayas in the Solukhumbu region of Nepal. It is a debris-free glacier and ranges from 4940 to 6420 masl (Sherpa et al., 2017). Similar to other glaciers in the Langtang and Solukhumbu regions, the climate of the Mera Glacier is dominated by the Indian summer monsoon. The record shows that nearly 80% of the total precipitation occurs during the summer season, while the rest takes place during the winter months

(Kaspari et al., 2014). The glaciological mass balance reported from both the glaciers, Yala and Mera, revealed that the mass balance of the Mera Glacier is less negative compared to the Yala Glacier (Acharya and Kayastha, 2018; Sherpa et al., 2017). The large portion of the total glacierized area located at higher elevations might be the most significant factor behind the minimal mass loss of the Mera Glacier (Acharya and Kayastha, 2018). As explained in the previous section, biomass burning was a predominant source of BC at the study site during the pre-monsoon season. We derived albedo reduction due to biomass BC (scenario 3) by considering 49% of observed BC in snow/ice. The albedo reduction was observed to be 0.77 which is 2.53% percent lower compared to BC free snow/ice. The mass loss was estimated at the rate of 3.07 kg m^{-2} per day which is 23% higher compared to BC free snow/ice conditions representing additional ablation at the rate of 0.57 kg m^{-2} per day. Our study could be characterized as more theoretical, thus providing an approach to calculate the extra mass loss caused by the BC present in the snowpack. The results might differ because the metamorphic property of snow was not considered, and the grains were considered spherical. Apart from that, during surface-mass-balance modeling, several parameterizations were used. The incoming energy fluxes were considered uniform over the whole glacier, and the shadowing effect of mountains was not considered. Besides, the aerodynamic roughness was taken as constant.

5. Conclusions

The annual mean ± standard deviation in situ atmospheric BC mass concentration was 0.42 ± 0.57 μg m^{-3}, with a maximum in the pre-monsoon season and the highest concentration observed in the month of April (1.12 ± 1.36 μg m^{-3}), while that from the model simulations overestimated the in situ results. The results may have a certain element of uncertainty, mainly related to the resolution of the model and the emission inventory (EDGAR version 2010) that we used in our study. The mean ± standard deviation BC and WIOC concentrations of surface snow during the campaign period were estimated to be 257 ± 111 ng g^{-1} and 460 ± 206 ng g^{-1}, respectively. The source apportionment study using AAE values for fresh ambient conditions indicates that the contribution of biomass burning to the BC mass during the entire study period was ~44% and that for April it was 49%, again indicating a higher contribution of biomass-burning aerosols in the pre-monsoon season. The model simulations suggest that Nepal and India together were responsible for contributing 69% to the total BC mass, followed by 22% from China, and the rest from the countries near the study site. The estimation of the scavenging ratio revealed a mean ± standard deviation value of 206 ± 72. The surface snow albedo reduction estimated via the online SNICAR model was in the range of 0.8–3.8% during the pre-monsoon season. The application of the simulation model of snow/glacier melt suggests melting in all seasons except winter, where a mass gain was observed. The glacier mass-balance analysis indicates that the BC generated from biomass-burning sources contributed approximately 23% to the total melting. This study also has certain limitations i.e. atmospheric BC measurements were conducted using optical methods whereas snow impurities were measured using thermo optical methods. Thus certain biases are expected while interpreting the results and determining scavenging ratios and BC, WIOC concentrations. Scientific evidences are required to understand BC/WIOC ratio in determining source contributions and aerosol ageing process influence on AAE for different sources. The WRF-Chem model simulations also need improvements over complex terrains.

Authors contribution

Chaman Gul: Data Curation, Writing - Original Draft, Writing - Review & Editing, Visualization, Formal analysis, Investigation. **Parth Sarathi Mahapatra**: Writing - Original Draft, Writing - Review & Editing, Investigation. **Mukesh Rai**: Data Curation, Visualization, Formal analysis. **Praveen Kumar Singh**: Writing - Review & Editing, Software. **Yangyang Xu**: Writing - Review & Editing, Methodology, Software, Conceptualization, Investigation. **Rajesh Kumar**: Writing - Review & Editing, Methodology, Software, Conceptualization, Investigation. **Shichang Kang**: Funding acquisition, Project administration, Resources. **Xiaokang Wu**: Software, Visualization, Validation. **Cenlin He**: Software, Visualization, Validation. **Siva Praveen Puppala**: Data Curation, Writing - Original Draft, Writing - Review & Editing, Formal analysis, Methodology, Conceptualization, Supervision, Project administration, Investigation.

Declaration of competing interest

The authors declare that they have no known competing financial interests or personal relationships that could have appeared to influence the work reported in this paper.

Acknowledgements

This study was partially supported by the core funds of ICIMOD contributed by the governments Afghanistan, Australia, Austria, Bangladesh, Bhutan, China, India, Myanmar, Nepal, Norway, Pakistan, Sweden, and Switzerland. The views and interpretations in this publication are those of the authors' and are not necessarily attributable to ICIMOD. It was also partially supported by the National Natural Science Foundation of China (41630754, 41671067, 41721091), the Chinese Academy of Sciences (XDA20040501, QYZDJ-SSW-DQC039), and the State Key Laboratory of Cryospheric Science (SKLCS-ZZ-2017). The National Center for Atmospheric Research is sponsored by the National Science Foundation. Thanks are due to Faiza Gul for technical support, and Shankar Prasad Paudel for providing the BC data. Cenlin He and Xiaokang Wu were supported by the NCAR Advanced Study Program (ASP) Fellowship. We thank Carmen Wickramagamage and Shanuj Vayot Cheruvakodan for the English-language editing of the manuscript. The authors would also like to convey their gratitude to the anonymous reviewers and the editor for their valuable comments and suggestions that have contributed immensely to improving the quality of this work.

Appendix A. Supplementary data

Supplementary data to this article can be found online at https://doi.org/10.1016/j.envpol.2021.116544.

References

Acharya, A., Kayastha, R.B., 2018. Mass and Energy Balance Estimation of Yala Glacier (2011-2017), Langtang Valley, Nepal. Water (Switzerland) 11. https://doi.org/10.3390/w11010006.

Ahmed, T., Dutkiewicz, V.A., Shareef, A., Tuncel, G., Tuncel, S., Husain, L., 2009. Measurement of black carbon (BC) by an optical method and a thermal-optical method: intercomparison for four sites. Atmos. Environ. 43, 6305–6311. https://doi.org/10.1016/j.atmosenv.2009.09.031.

Anslow, F.S., Hostetler, S., Bidlake, W.R., Clark, P.U., 2008. Distributed energy balance modeling of South Cascade Glacier, Washington and assessment of model uncertainty. J. Geophys. Res. Earth Surf. 113, 1–18. https://doi.org/10.1029/2007JF000850.

Armalis, S., 1999. Wet deposition of elemental carbon in Lithuania. Sci. Total Environ. 239, 89–93. https://doi.org/10.1016/S0048-9697(99)00288-0.

Azam, M.F., Wagnon, P., Vincent, C., Ramanathan, A., Mandal, A., Pottakkal, J.G.,

2014. Processes governing the mass balance of Chhota Shigri Glacier (Western Himalaya, India) assessed by point-scale surface energy balance measurements. Cryosphere Discuss. 8, 2867–2922. https://doi.org/10.5194/tcd-8-2867-2014.

Babu, S.S., Chaubey, J.P., Krishna Moorthy, K., Gogoi, M.M., Kompalli, S.K., Sreekanth, V., Bagare, S.P., Bhatt, B.C., Gaur, V.K., Prabhu, T.P., Singh, N.S., 2011. High altitude (~4520 m amsl) measurements of black carbon aerosols over western trans-Himalayas: seasonal heterogeneity and source apportionment. J. Geophys. Res. Atmos. 116, 1–15. https://doi.org/10.1029/2011JD016722.

Baltensperger, U., Gäggeler, H.W., Jost, D.T., Lugauer, M., Schwikowski, M., Weingartner, E., Seibert, P., 1997. Aerosol climatology at the high-alpine site Jungfraujoch, Switzerland. J. Geophys. Res. Atmos. 102, 19707–19715.

Blanco-Alegre, C., Calvo, A.I., Coz, E., Castro, A., Oduber, F., Prévôt, A.S.H., Močnik, G., Fraile, R., 2019. Quantification of source specific black carbon scavenging using an aethalometer and a disdrometer. Environ. Pollut. 246, 336–345. https://doi.org/10.1016/j.envpol.2018.11.102.

Bonasoni, P., Cristofanelli, P., Marinoni, A., Pradhan, B.B., Fuzzi, S., Gobbi, G.P., 2010. High Concentration of Black Carbon Observed in the High Himalayas Editorial: Black Carbon and the Third Pole Testimony on Black Carbon, vol. 2, pp. 1–4.

Bond, T.C., Doherty, S.J., Fahey, D.W., Forster, P.M., Berntsen, T., Deangelo, B.J., Flanner, M.G., Ghan, S., Kärcher, B., Koch, D., Kinne, S., Kondo, Y., Quinn, P.K., Sarofim, M.C., Schultz, M.G., Schulz, M., Venkataraman, C., Zhang, H., Zhang, S., Bellouin, N., Guttikunda, S.K., Hopke, P.K., Jacobson, M.Z., Kaiser, J.W., Klimont, Z., Lohmann, U., Schwarz, J.P., Shindell, D., Storelvmo, T., Warren, S.G., Zender, C.S., 2013. Bounding the role of black carbon in the climate system: a scientific assessment. J. Geophys. Res. Atmos. 118, 5380–5552. https://doi.org/10.1002/jgrd.50171.

Bond, T.C., Streets, D.G., Yarber, K.F., Nelson, S.M., Woo, J.H., Klimont, Z., 2004. A technology-based global inventory of black and organic carbon emissions from combustion. J. Geophys. Res. Atmos. 109, 1–43. https://doi.org/10.1029/2003JD003697.

Braun, M., Hock, R., 2004. Spatially distributed surface energy balance and ablation modelling on the ice cap of King George Island (Antarctica). Global Planet. Change 42, 45–58. https://doi.org/10.1016/j.gloplacha.2003.11.010.

Carrico, C.M., Bergin, M.H., Shrestha, A.B., Dibb, J.E., Gomes, L., Harris, J.M., 2003. The importance of carbon and mineral dust to seasonal aerosol properties in the Nepal Himalaya. Atmos. Environ. 37 (20), 2811–2824. https://doi.org/10.1016/S1352-2310(03)00197-3.

Cereceda-Balic, F., Gorena, T., Soto, C., Vidal, V., Lapuerta, M., Moosmüller, H., 2019. Optical determination of black carbon mass concentrations in snow samples: a new analytical method. Sci. Total Environ. 697, 133934. https://doi.org/10.1016/j.scitotenv.2019.133934.

Chaubey, J.P., Babu, S.S., Gogoi, M.M., Kompalli, S.K., Sreekanth, V., Moorthy, K.K., Prabhu, T.P., 2012. Black carbon aerosol over a high altitude (~ 4.52 km) station in western Indian Himalayas. J. Inst. Eng. 8, 42–51. https://doi.org/10.3126/jie.v8i3.5930.

Chen, X., Kang, S., Cong, Z., Yang, J., Ma, Y., 2018. Concentration, temporal variation, and sources of black carbon in the Mt. Everest region retrieved by real-time observation and simulation. Atmos. Chem. Phys. 18, 12859–12875. https://doi.org/10.5194/acp-18-12859-2018.

Dahal, N., Shrestha, U.B., Tuitui, A., Ojha, H.R., 2019. Temporal changes in precipitation and temperature and their implications on the streamflow of Rosi river, Central Nepal. Climate 7, 1–15. https://doi.org/10.3390/cli7010003.

Dhungel, S., Kathayat, B., Mahata, K., Panday, A., 2018. Transport of regional pollutants through a remote trans-Himalayan valley in Nepal. Atmos. Chem. Phys. 18, 1203–1216. https://doi.org/10.5194/acp-18-1203-2018.

Drinovec, L., Močnik, G., Zotter, P., Prévôt, A.S.H., Ruckstuhl, C., Coz, E., Rupakheti, M., Sciare, J., Müller, T., Wiedensohler, A., Hansen, A.D.A., 2015. The "dual-spot" Aethalometer: an improved measurement of aerosol black carbon with real-time loading compensation. Atmos. Meas. Tech. 8, 1965–1979. https://doi.org/10.5194/amt-8-1965-2015.

Flanner, M.G., Zender, C.S., Hess, P.G., Mahowald, N.M., Painter, T.H., Ramanathan, V., Rasch, P.J., 2009. Springtime warming and reduced snow cover from carbonaceous particles. Atmos. Chem. Phys. 9 (7), 2481–2497. https://doi.org/10.5194/acp-9-2481-2009.

Flanner, M.G., Zender, C.S., Randerson, J.T., Rasch, P.J., 2007. Present-day climate forcing and response from black carbon in snow. J. Geophys. Res. Atmos. 112 (D11) https://doi.org/10.1029/2006JD008003.

Giesen, R.H., Andreassen, L.M., Oerlemans, J., Van Den Broeke, M.R., 2014. Surface energy balance in the ablation zone of Langfjordjøkelen, an arctic, maritime glacier in northern Norway. J. Glaciol. 60, 57–70. https://doi.org/10.3189/2014JoG13J063.

Ginot, P., Dumont, M., Lim, S., Patris, N., Taupin, J.D., Wagnon, P., Gilbert, A., Arnaud, Y., Marinoni, A., Bonasoni, P., Laj, P., 2014. A 10 year record of black carbon and dust from a Mera Peak ice core (Nepal): variability and potential impact on melting of Himalayan glaciers. Cryosphere 8, 1479–1496. https://doi.org/10.5194/tc-8-1479-2014.

Granat, L., Engström, J.E., Praveen, S., Rodhe, H., 2010. Light absorbing material (soot) in rainwater and in aerosol particles in the Maldives. J. Geophys. Res. Atmos. 115, 1–12. https://doi.org/10.1029/2009JD013768.

Grell, G.A., Peckham, S.E., Schmitz, R., McKeen, S.A., Frost, G., Skamarock, W.C., Eder, B., 2005. Fully coupled chemistry within the WRF model. Atmos. Environ. 39, 6957–6975. https://doi.org/10.1016/j.atmosenv.2005.04.027.

Guenther, A.B., Jiang, X., Heald, C.L., Sakulyanontvittaya, T., Duhl, T., Emmons, L.K., Wang, X., 2012. The Model of Emissions of Gases and Aerosols from Nature version 2.1 (MEGAN2.1): an extended and updated framework for modeling biogenic emissions. Geosci. Model Dev. (GMD) 5, 1471–1492. https://doi.org/10.5194/gmd-5-1471-2012.

Gul, C., Puppala, S.P., Kang, S., Adhikary, B., Zhang, Y., Ali, S., Li, Y., Li, X., 2018. Concentrations and source regions of light-absorbing particles in snow/ice in northern Pakistan and their impact on snow albedo. Atmos. Chem. Phys. 18, 4981–5000. https://doi.org/10.5194/acp-18-4981-2018.

Gustafsson, Ö., Ramanathan, V., 2016. Convergence on climate warming by black carbon aerosols. Proc. Natl. Acad. Sci. U. S. A 113 (16), 4243–4245. https://doi.org/10.1073/pnas.1603570113.

He, C., Chen, F., Barlage, M., Liu, C., Newman, A., Tang, W., Ikeda, K., Rasmussen, R., 2019. Can convection-permitting modeling provide decent precipitation for offline high-resolution snowpack simulations over mountains? J. Geophys. Res. Atmos. 124 (23), 12631–12654. https://doi.org/10.1029/2019JD030823.

He, C., Flanner, M.G., Chen, F., Barlage, M., Liou, K.N., Kang, S., Ming, J., Qian, Y., 2018. Black carbon-induced snow albedo reduction over the Tibetan Plateau: uncertainties from snow grain shape and aerosol-snow mixing state based on an updated SNICAR model. Atmos. Chem. Phys. 18 (15), 11507–11527. https://doi.org/10.5194/acp-18-11507-2018.

He, Cenlin, Li, Q., Liou, K.N., Takano, Y., Gu, Y., Qi, L., Mao, Y., Leung, L.R., 2014a. Black carbon radiative forcing over the Tibetan Plateau. Geophys. Res. Lett. 41 (22), 7806–7813. https://doi.org/10.1002/2014GL062191.

He, C., Li, Q.B., Liou, K.N., Zhang, J., Qi, L., Mao, Y., Gao, M., Lu, Z., Streets, D.G., Zhang, Q., Sarin, M.M., Ram, K., 2014b. A global 3-D CTM evaluation of black carbon in the Tibetan Plateau. Atmos. Chem. Phys. 14 (13), 7091–7112. https://doi.org/10.5194/acp-14-7091-2014.

Hegg, D.A., Clarke, A.D., Doherty, S.J., Ström, J., 2011. Measurements of black carbon aerosol washout ratio on Svalbard. Tellus Ser. B Chem. Phys. Meteorol. 63, 891–900. https://doi.org/10.1111/j.1600-0889.2011.00577.x.

Hock, R., Holmgren, B., 2005. A distributed surface energy-balance model for complex topography and its application to Storglaciären, Sweden. J. Glaciol. 51, 25–36.

Ikeda, K., Tanimoto, H., Sugita, T., Akiyoshi, H., Kanaya, Y., Zhu, C., Taketani, F., 2017. Tagged tracer simulations of black carbon in the Arctic: transport, source contributions, and budget. Atmos. Chem. Phys. 17 (17), 10515–10533. https://doi.org/10.5194/acp-17-10515-2017.

Jacobson, M.Z., 2004. Climate response of fossil fuel and biofuel soot, accounting for soot's feedback to snow and sea ice albedo and emissivity. J. Geophys. Res. Atmos. 109 https://doi.org/10.1029/2004JD004945 n/a-n/a.

Kang, S., Zhang, Q., Qian, Y., Ji, Z., Li, C., Cong, Z., Zhang, Y., Guo, J., Du, W., Huang, J., You, Q., Panday, A.K., Rupakheti, M., Chen, D., Gustafsson, Ö., Thiemens, M.H., Qin, D., 2019. Linking atmospheric pollution to cryospheric change in the Third Pole region: current progress and future prospects. Natl. Sci. Rev. 6 (4), 796–809. https://doi.org/10.1093/nsr/nwz031.

Kaspari, S., Painter, T.H., Gysel, M., Skiles, S.M., Schwikowski, M., 2014. Seasonal and elevational variations of black carbon and dust in snow and ice in the Solu-Khumbu, Nepal and estimated radiative forcings. Atmos. Chem. Phys. 14, 8089–8103. https://doi.org/10.5194/acp-14-8089-2014.

Kayastha, R.B., Ohata, T., Ageta, Y., 1999. Application of a mass-balance model to a Himalayan glacier. J. Glaciol. 45, 559–567.

Kirchstetter, T.W., Novakov, T., Hobbs, P.V., 2004. Evidence that the spectral dependence of light absorption by aerosols is affected by organic carbon. J. Geophys. Res. 109, D21208. https://doi.org/10.1029/2004JD004999.

Klok, E.J., Nolan, M., Van Den Broeke, M.R., 2005. Analysis od meteorological data and the surface energy balance of McCall Glacier, Alaska, USA. J. Glaciol. 51, 451–461. https://doi.org/10.3189/172756505781829241.

Knote, C., Hodzic, A., Jimenez, J.L., Volkamer, R., Orlando, J.J., Baidar, S., Brioude, J., Fast, J., Gentner, D.R., Goldstein, A.H., Hayes, P.L., Knighton, W.B., Oetjen, H., Setyan, A., Stark, H., Thalman, R., Tyndall, G., Washenfelder, R., Waxman, E., Zhang, Q., 2014. Simulation of semi-explicit mechanisms of SOA formation from glyoxal in aerosol in a 3-D model. Atmos. Chem. Phys. 14 (12), 6213–6239. https://doi.org/10.5194/acp-14-6213-2014.

Krecl, P., de Lima, C.H., Dal Bosco, T.C., Targino, A.C., Hashimoto, E.M., Oukawa, G.Y., 2020. Open waste burning causes fast and sharp changes in particulate concentrations in peripheral neighborhoods. Sci. Total Environ. 142736 https://doi.org/10.1016/j.scitotenv.2020.142736.

Kumar, R., Barth, M.C., Pfister, G.G., Nair, V.S., Ghude, S.D., Ojha, N., 2015. What controls the seasonal cycle of black carbon aerosols in India? J. Geophys. Res. Atmos. 120, 7788–7812. https://doi.org/10.1002/2015JD023298.

Lack, D.A., Moosmüller, H., McMeeking, G.R., Chakrabarty, R.K., Baumgardner, D., 2014. Characterizing elemental, equivalent black, and refractory black carbon aerosol particles: a review of techniques, their limitations and uncertainties. Anal. Bioanal. Chem. 406 (1), 99–122. https://doi.org/10.1007/s00216-013-7402-3.

Li, C., Bosch, C., Kang, S., Andersson, A., Chen, P., Zhang, Q., Cong, Z., Chen, B., Qin, D., Gustafsson, Ö., 2016a. Sources of black carbon to the Himalayan-Tibetan Plateau glaciers. Nat. Commun. 7, 1–7. https://doi.org/10.1038/ncomms12574.

Li, C., Yan, F., Kang, S., Chen, P., Han, X., Hu, Z., Zhang, G., Hong, Y., Gao, S., Qu, B., Zhu, Z., Li, J., Chen, B., Sillanpaä, M., 2017. Re-evaluating black carbon in the Himalayas and the Tibetan Plateau: concentrations and deposition. Atmos. Chem. Phys. 17 (19), 11899–11912. https://doi.org/10.5194/acp-17-11899-2017.

Li, X., Kang, S., He, X., Qu, B., Tripathee, L., Jing, Z., Paudyal, R., Li, Y., Zhang, Y., Yan, F., Li, G., Li, C., 2017. Light-absorbing impurities accelerate glacier melt in the Central Tibetan Plateau. Sci. Total Environ. 482–490. https://doi.org/10.1016/j.scitotenv.2017.02.169.

Li, X., Kang, S., Zhang, G., Qu, B., Tripathee, L., Paudyal, R., Jing, Z., Zhang, Y., Yan, F.,

Li, G., Cui, X., Xu, R., Hu, Z., Li, C., 2018. Light-absorbing impurities in a southern Tibetan Plateau glacier: variations and potential impact on snow albedo and radiative forcing. Atmos. Res. 200, 77–87. https://doi.org/10.1016/j.atmosres.2017.10.002.

Li, Y., Chen, J., Kang, S., Li, C., Qu, B., Tripathee, L., Yan, F., Zhang, Y., Guo, J., Gul, C., Qin, X., 2016b. Impacts of black carbon and mineral dust on radiative forcing and glacier melting during summer in the Qilian Mountains, northeastern Tibetan Plateau. Cryosphere Discuss. 1–14. https://doi.org/10.5194/tc-2016-32.

Liu, C., Chung, C.E., Yin, Y., Schnaiter, M., 2018. The absorption Ångström exponent of black carbon: from numerical aspects. Atmos. Chem. Phys. 18, 6259–6273. https://doi.org/10.5194/acp-18-6259-2018.

Liu, C., Chung, C.E., Zhang, F., Yin, Y., 2016. The colors of biomass burning aerosols in the atmosphere. Sci. Rep. 6, 28267. https://doi.org/10.1038/srep28267.

Liu, L., Ma, Y., Menenti, M., Zhang, X., Ma, W., 2019. Evaluation of WRF modeling in relation to different land surface schemes and initial and boundary conditions: a snow event simulation over the Tibetan plateau. J. Geophys. Res. Atmos. 124 (1), 209–226. https://doi.org/10.1029/2018JD029208.

Liu, S., Aiken, A.C., Gorkowski, K., Dubey, M.K., Cappa, C.D., Williams, L.R., Herndon, S.C., Massoli, P., Fortner, E.C., Chhabra, P.S., Brooks, W.A., Onasch, T.B., Jayne, J.T., Worsnop, D.R., China, S., Sharma, N., Mazzoleni, C., Xu, L., Ng, N.L., Liu, D., Allan, J.D., Lee, J.D., Fleming, Z.L., Mohr, C., Zotter, P., Szidat, S., Prévôt, A.S.H., 2015. Enhanced light absorption by mixed source black and brown carbon particles in UK winter. Nat. Commun. 6 https://doi.org/10.1038/ncomms9435.

Marcq, S., Laj, P., Roger, J.C., Villani, P., Sellegri, K., Bonasoni, P., Marinoni, A., Cristofanelli, P., Verza, G.P., Bergin, M., 2010. Aerosol optical properties and radiative forcing in the high Himalaya based on measurements at the Nepal Climate Observatory-Pyramid site (5079 m a.s.l.). Atmos. Chem. Phys. 10, 5859–5872. https://doi.org/10.5194/acp-10-5859-2010.

Marinoni, A., Cristofanelli, P., Laj, P., Duchi, R., Calzolari, F., Decesari, S., Sellegri, K., Vuillermoz, E., Verza, G.P., Villani, P., Bonasoni, P., 2010. Aerosol mass and black carbon concentrations, a two year record at NCO-P (5079 m, Southern Himalayas). Atmos. Chem. Phys. 10, 8551–8562. https://doi.org/10.5194/acp-10-8551-2010.

Marinoni, A., Cristofanelli, P., Laj, P., Duchi, R., Putero, D., Calzolari, F., Landi, T.C., Vuillermoz, E., Maione, M., Bonasoni, P., 2013. High black carbon and ozone concentrations during pollution transport in the Himalayas: five years of continuous observations at NCO-P global GAW station. J. Environ. Sci. (China) 25 (8). https://doi.org/10.1016/S1001-0742(12)60242-3.

Ming, J., Xiao, C., Cachier, H., Qin, D., Qin, X., Li, Z., Pu, J., 2009. Black Carbon (BC) in the snow of glaciers in west China and its potential effects on albedos. Atmos. Res. 92 (1), 114–123. https://doi.org/10.1016/j.atmosres.2008.09.007.

Ming, J., Xiao, C., Du, Z., Yang, X., 2013. An overview of black carbon deposition in High Asia glaciers and its impacts on radiation balance. Adv. Water Resour. 55, 80–87. https://doi.org/10.1016/j.advwatres.2012.05.015.

Nair, V.S., Babu, S.S., Moorthy, K.K., Sharma, A.K., Marinoni, A., Ajai, 2013. Black carbon aerosols over the Himalayas: direct and surface albedo forcing. Tellus B 65. https://doi.org/10.3402/tellusb.v65i0.19738, 19738.

Niu, H., Kang, S., Wang, H., Du, J., Pu, T., Zhang, G., Lu, X., Yan, X., Wang, S., Shi, X., 2019. Light-absorbing impurities accelerating glacial melting in southeastern Tibetan Plateau. Environ. Pollut. 113541 https://doi.org/10.1016/j.envpol.2019.113541.

Niu, H., Kang, S., Wang, Y., Sarangi, C., Rupakheti, D., Qian, Y., 2020. Measurements of light-absorbing impurities in snow over four glaciers on the Tibetan Plateau. Atmos. Res. 243 https://doi.org/10.1016/j.atmosres.2020.105002.

Noone, K.J., Clarke, A.D., 1988. Soot scavenging measurements in Arctic snowfall. Atmos. Environ. 22, 2773–2778. https://doi.org/10.1016/0004-6981(88)90444-1.

Pellicciotti, F., Helbing, J., Rivera, A., Favier, V., Corripio, J., Araos, J., Sicart, J.-E., Carenzo, M., 2008. A study of the energy balance and melt regime on Juncal Norte Glacier, semi-arid Andes of central Chile, using melt models of different complexity. Hydrol. Process. 22, 3980–3997. https://doi.org/10.1002/hyp.7085.

Petzold, A., Ogren, J.A., Fiebig, M., Laj, P., Li, S.M., Baltensperger, U., Holzer-Popp, T., Kinne, S., Pappalardo, G., Sugimoto, N., Wehrli, C., Wiedensohler, A., Zhang, X.Y., 2013. Recommendations for reporting black carbon measurements. Atmos. Chem. Phys. 13 (16), 8365–8379. https://doi.org/10.5194/acp-13-8365-2013.

Putero, D., Landi, T.C., Cristofanelli, P., Marinoni, A., Laj, P., Duchi, R., Calzolari, F., Verza, G.P., Bonasoni, P., 2014. Influence of open vegetation fires on black carbon and ozone variability in the southern Himalayas (NCO-P, 5079 m a.s.l.). Environ. Pollut. 184, 597–604. https://doi.org/10.1016/j.envpol.2013.09.035.

Putero, D., Marinoni, A., Calzolari, F., Rupakheti, M., Cristofanelli, P., Bonasoni, P., 2018. Black carbon and ozone variability at the kathmandu valley and at the southern Himalayas: a comparison between a “hot spot” and a downwind high-altitude site. Aerosol Air Qual. Res. 18, 623–635. https://doi.org/10.4209/aaqr.2017.04.0138.

Qian, Y., Yasunari, T.J., Doherty, S.J., Flanner, M.G., Lau, W.K.M., Ming, J., Wang, H., Wang, M., Warren, S.G., Zhang, R., 2015. Light-absorbing particles in snow and ice: measurement and modeling of climatic and hydrological impact. Adv. Atmos. Sci. 32, 64–91. https://doi.org/10.1007/s00376-014-0010-0.

Rai, M., Mahapatra, P.S., Gul, C., Kayastha, R.B., Panday, A.K., Puppala, S.P., 2019. Aerosol radiative forcing estimation over a remote high-altitude location (~4900 masl) near Yala glacier, Nepal. Aerosol Air Qual. Res. 19, 1872–1891. https://doi.org/10.4209/aaqr.2018.09.0342.

Ram, K., Sarin, M.M., Hegde, P., 2010. Long-term record of aerosol optical properties and chemical composition from a high-altitude site (Manora Peak) in Central Himalaya. Atmos. Chem. Phys. 10 (23), 11791–11803. https://doi.org/10.5194/acp-10-11791-2010.

Ram, K., Sarin, M.M., Hegde, P., 2008. Atmospheric abundances of primary and secondary carbonaceous species at two high-altitude sites in India: sources and temporal variability. Atmos. Environ. 42, 6785–6796. https://doi.org/10.1016/j.atmosenv.2008.05.031.

Reijmer, C.H., Hock, R., 2008. Internal accumulation on Storglaciären, Sweden, in a multi-layer snow model coupled to a distributed energy-and mass-balance model. J. Glaciol. 54, 61–72.

Romonosky, D.E., Gomez, S.L., Lam, J., Carrico, C.M., Aiken, A.C., Chylek, P., Dubey, M.K., 2019. Optical properties of laboratory and ambient biomass burning aerosols: elucidating black, Brown, and organic carbon components and mixing regimes. J. Geophys. Res.: Atmosphere 124 (9), 5088–5105. https://doi.org/10.1029/2018JD029892.

Sandradewi, J., Prévôt, A.S.H., Weingartner, E., Schmidhauser, R., Gysel, M., Baltensperger, U., 2008. A study of wood burning and traffic aerosols in an Alpine valley using a multi-wavelength Aethalometer. Atmos. Environ. 42, 101–112. https://doi.org/10.1016/j.atmosenv.2007.09.034.

Santra, S., Verma, S., Fujita, K., Chakraborty, I., Boucher, O., Takemura, T., Burkhart, J.F., Matt, F., Sharma, M., 2019. Simulations of black carbon (BC) aerosol impact over Hindu Kush Himalayan sites: validation, sources, and implications on glacier runoff. Atmos. Chem. Phys. 19, 2441–2460. https://doi.org/10.5194/acp-19-2441-2019.

Sarangi, C., Qian, Y., Rittger, K., Bormann, K.J., Liu, Y., Wang, H., Wan, H., Lin, G., Painter, T.H., 2019. Impact of light-absorbing particles on snow albedo darkening and associated radiative forcing over high-mountain Asia: high-resolution WRF-Chem modeling and new satellite observations. Atmos. Chem. Phys. 19, 7105–7128. https://doi.org/10.5194/acp-19-7105-2019.

Schwarz, J.P., Doherty, S.J., Li, F., Ruggiero, S.T., Tanner, C.E., Perring, A.E., Gao, R.S., Fahey, D.W., 2012. Assessing single particle soot photometer and integrating sphere/integrating sandwich spectrophotometer measurement techniques for quantifying black carbon concentration in snow. Atmos. Meas. Tech. 5, 2581–2592. https://doi.org/10.5194/amt-5-2581-2012.

Scott, C.A., Zhang, F., Mukherji, A., Immerzeel, W., Mustafa, D., Bharati, L., 2019. The Hindu Kush Himalaya Assessment, the Hindu Kush Himalaya Assessment. Springer International Publishing. https://doi.org/10.1007/978-3-319-92288-1.

Shea, J.M., Wagnon, P., Immerzeel, W.W., Biron, R., Brun, F., Pellicciotti, F., 2015. A comparative high-altitude meteorological analysis from three catchments in the Nepalese Himalaya. Int. J. Water Resour. Dev. 31, 174–200. https://doi.org/10.1080/07900627.2015.1020417.

Sherpa, S.F., Wagnon, P., Brun, F., Berthier, E., Vincent, C., Lejeune, Y., Arnaud, Y., Kayastha, R.B., Sinisalo, A., 2017. Contrasted surface mass balances of debris-free glaciers observed between the southern and the inner parts of the Everest region (2007-15). J. Glaciol. 63, 637–651. https://doi.org/10.1017/jog.2017.30.

Sicart, J.E., Hock, R., Ribstein, P., Litt, M., Ramirez, E., 2011. Analysis of seasonal variations in mass balance and meltwater discharge of the tropical Zongo Glacier by application of a distributed energy balance model. J. Geophys. Res. Atmos. 116, 1–18. https://doi.org/10.1029/2010JD015105.

Sicart, J.E., Hock, R., Six, D., 2008. Glacier melt, air temperature, and energy balance in different climates: the Bolivian Tropics, the French Alps, and northern Sweden. J. Geophys. Res. Atmos. 113, 1–11. https://doi.org/10.1029/2008JD010406.

Targino, A.C., Coe, H., Cozic, J., Crosier, J., Crawford, I., Bower, K., Flynn, M., Gallagher, M., Allan, J., Verheggen, B., Weingartner, E., Baltensperger, U., Choularton, T., 2009. Influence of particle chemical composition on the phase of cold clouds at a high-alpine site in Switzerland. J. Geophys. Res. Atmos. 114 https://doi.org/10.1029/2008JD011365. D18206.

Wang, Y., Chung, A., Paulson, S.E., 2010. The effect of metal salts on quantification of elemental and organic carbon in diesel exhaust particles using thermal-optical evolved gas analysis. Atmos. Chem. Phys. 10 (23), 11447–11457. https://doi.org/10.5194/acp-10-11447-2010.

Wang, Y., Ma, P.L., Peng, J., Zhang, R., Jiang, J.H., Easter, R.C., Yung, Y.L., 2018. Constraining aging processes of black carbon in the community atmosphere model using environmental chamber measurements. J. Adv. Model. Earth Syst. 10 (10), 2514–2526. https://doi.org/10.1029/2018MS001387.

Wendl, I.A., Menking, J.A., Färber, R., Gysel, M., Kaspari, S.D., Laborde, M.J.G., Schwikowski, M., 2014. Optimized method for black carbon analysis in ice and snow using the Single Particle Soot Photometer. Atmos. Meas. Tech. 7 (8), 2667–2681. https://doi.org/10.5194/amt-7-2667-2014.

Wu, C., Huang, X.H.H., Ng, W.M., Griffith, S.M., Yu, J.Z., 2016. Inter-comparison of NIOSH and IMPROVE protocols for OC and EC determination: implications for inter-protocol data conversion. Atmos. Meas. Tech. 9, 4547–4560. https://doi.org/10.5194/amt-9-4547-2016.

Xu, B., Cao, J., Hansen, J., Yao, T., Joswia, D.R., Wang, N., Wu, G., Wang, M., Zhao, H., Yang, W., Liu, X., He, J., 2009. Black soot and the survival of Tibetan glaciers. Proc. Natl. Acad. Sci. U. S. A 106 (52), 22114–22118. https://doi.org/10.1073/pnas.0910444106.

Yasunari, T.J., Bonasoni, P., Laj, P., Fujita, K., Vuillermoz, E., Marinoni, A., Cristofanelli, P., Duchi, R., Tartari, G., Lau, K.-M., 2010. Estimated impact of black carbon deposition during pre-monsoon season from Nepal Climate Observatory – pyramid data and snow albedo changes over Himalayan glaciers. Atmos. Chem. Phys. 10, 6603–6615. https://doi.org/10.5194/acp-10-6603-2010.

Yasunari, T.J., Tan, Q., Lau, K.M., Bonasoni, P., Marinoni, A., Laj, P., Ménégoz, M., Takemura, T., Chin, M., 2013. Estimated range of black carbon dry deposition and the related snow albedo reduction over Himalayan glaciers during dry pre-

monsoon periods. Atmos. Environ. 78, 259–267. https://doi.org/10.1016/j.atmosenv.2012.03.031.

Zaveri, R.A., Easter, R.C., Fast, J.D., Peters, L.K., 2008. Model for simulating aerosol Interactions and chemistry (MOSAIC). J. Geophys. Res. Atmos. 113 (D13) https://doi.org/10.1029/2007JD008782.

Zhang, C., Guo, Y., Xiao, X., Bloom, M.S., Qian, Z., Rolling, C.A., Xian, H., Lin, S., Li, S., Chen, G., Jalava, P., Roponen, M., Hirvonen, M.-R., Komppula, M., Leskinen, A., Yim, S.H.L., Chen, D.-H., Ma, H., Zeng, X.-W., Hu, L.-W., Liu, K.-K., Yang, B.-Y., Dong, G.-H., 2019. Association of breastfeeding and air pollution exposure with lung function in Chinese children. JAMA Netw. Open 2, e194186. https://doi.org/10.1001/jamanetworkopen.2019.4186.

Zhang, G., Kang, S., Fujita, K., Huintjes, E., Xu, J., Yamazaki, T., Haginoya, S., Wei, Y., Scherer, D., Schneider, C., Yao, T., 2013. Energy and mass balance of Zhadang glacier surface, central Tibetan Plateau. J. Glaciol. 59, 137–148. https://doi.org/10.3189/2013JoG12J152.

Zhang, R., Wang, H., Qian, Y., Rasch, P.J., Easter, R.C., Ma, P.L., Singh, B., Huang, J., Fu, Q., 2015. Quantifying sources, transport, deposition, and radiative forcing of black carbon over the Himalayas and Tibetan Plateau. Atmos. Chem. Phys. 15 (11), 6205–6223. https://doi.org/10.5194/acp-15-6205-2015.

Zhang, Y., Kang, S., Cong, Z., Schmale, J., Sprenger, M., Li, C., Yang, W., Gao, T., Sillanpää, M., Li, X., Liu, Y., Chen, P., Zhang, X., 2017. Light-absorbing impurities enhance glacier albedo reduction in the southeastern Tibetan plateau. J. Geophys. Res. 122 (13), 6915–6933. https://doi.org/10.1002/2016JD026397.

Zhang, Y., Kang, S., Sprenger, M., Cong, Z., Gao, T., Li, C., Tao, S., Li, X., Zhong, X., Xu, M., Meng, W., Neupane, B., Qin, X., Sillanpää, M., 2018. Black carbon and mineral dust in snow cover on the Tibetan Plateau. Cryosphere 12 (2), 413–431. https://doi.org/10.5194/tc-12-413-2018.

Zhang, A., Wang, Y., Zhang, Y., J Weber, R., Song, Y., Ke, Z., Zou, Y., 2020. Modeling the global radiative effect of brown carbon: a potentially larger heating source in the tropical free troposphere than black carbon. Atmos. Chem. Phys. 20 (4), 1901–1920. https://doi.org/10.5194/acp-20-1901-2020.

Zotter, P., Herich, H., Gysel, M., El-Haddad, I., Zhang, Y., Mocnik, G., Hüglin, C., Baltensperger, U., Szidat, S., Prévôt, A.S.H., 2017. Evaluation of the absorption Ångström exponents for traffic and wood burning in the Aethalometer-based source apportionment using radiocarbon measurements of ambient aerosol. Atmos. Chem. Phys. 17 (6), 4229–4249. https://doi.org/10.5194/acp-17-4229-2017.